

Article

Molten Bismuth–Bismuth/Zinc Oxide Composites for High-Temperature Thermal Energy Storage

Cristina Maria Vladut ¹, Daniel Lincu ¹, Daniela Berger ², Cristian Matei ² and Raul-Augustin Mitran ^{1,*}

¹ “Ilie Murgulescu” Institute of Physical Chemistry, Romanian Academy, 202 Splaiul Independentei, 060021 Bucharest, Romania; vladut@icf.ro (C.M.V.)

² Faculty of Chemical Engineering and Biotechnology, University “Politehnica” of Bucharest, 1-7 Polizu Street, 011061 Bucharest, Romania; cristi_matei@yahoo.com (C.M.)

* Correspondence: raul.mitran@gmail.com

Abstract: Thermal energy storage is at the leading edge of various applications, including waste heat recovery, solar storage and zero-energy buildings. Phase change materials (PCMs) can be utilized to store heat through reversible solid–liquid phase transitions. PCMs provide high energy storage capacity at a constant temperature. The volume change during the phase transition, on the other hand, causes inconsistency in crystallization and leakage, increasing the system’s complexity and shortening the lifetime of these materials. These shortcomings can be diminished by impregnation in a porous matrix or encapsulation with an inert shell, resulting in shape-stabilized PCMs that maintain their macroscopic shape during phase change. The synthesis and properties of Bi/ZnO nanocomposites were investigated in order to obtain shape-stabilized phase change materials. All samples consisted of metallic Bi and oxide, doped with 1–3% at. zinc. Heat storage capacities between 31 and 49 Jg^{−1} were obtained, depending on the mass fraction of the metal. All samples had good thermal reliability, retaining their heat storage properties after 50 consecutive heating–cooling cycles. An average oxide layer thickness of 75–100 nm is sufficient to prevent the molten metal leakage at temperatures above its melting point, resulting in shape-stabilized PCMs.

Keywords: phase change materials; shape stabilized; zinc oxide; bismuth



Citation: Vladut, C.M.; Lincu, D.; Berger, D.; Matei, C.; Mitran, R.-A. Molten Bismuth–Bismuth/Zinc Oxide Composites for High-Temperature Thermal Energy Storage. *Inorganics* **2024**, *12*, 126. <https://doi.org/10.3390/inorganics12050126>

Academic Editor: Roberto Nisticò

Received: 29 February 2024

Revised: 18 April 2024

Accepted: 19 April 2024

Published: 23 April 2024



Copyright: © 2024 by the authors. Licensee MDPI, Basel, Switzerland. This article is an open access article distributed under the terms and conditions of the Creative Commons Attribution (CC BY) license (<https://creativecommons.org/licenses/by/4.0/>).

1. Introduction

Thermal energy storage at elevated temperatures (>200 °C) is of growing importance to both industrial processes and solar energy storage and generation [1]. Thermal energy can be stored as sensible, latent or chemical energy [2]. Latent heat storage offers near-constant operating temperatures, good heat storage capacity and low system complexity in comparison with the other two approaches [3,4]. Latent heat is typically stored through phase transitions between solid and liquid phases. The materials used for latent heat storage are called phase change materials (PCMs). Latent heat storage can also be combined with sensible storage, increasing the energy storage capacity and operating range [5].

Both organic and inorganic substances can act as PCMs, provided that they have high phase transition enthalpy at a useful temperature, chemical stability and a low cost [6–8]. Pure substances suffer, however, from some drawbacks, which arise from the change in molar volume during phase transition [9,10]. The change in molar volume during phase transition can lead to leakage, a decreased thermal transfer surface area, loss of heat storage or installation damage during operation. These drawbacks can be mitigated by creating so-called shape-stabilized PCMs, which are composites that retain their macroscopic solid shape at temperatures above the melting point of the active heat storage phase [11–13]. Shape-stabilized PCMs contain either a protective, inert shell or a high-porosity matrix.

Metals and metallic compounds are attractive phase change materials for high-temperature (>200 °C) applications due to their high density and volumetric heat storage capacity and large thermal conductivity values [14,15]. Metallic Zn microparticles were

encapsulated with oxide shells (TiO_2 , Al_2O_3 , SiO_2) in order to create shape-stabilized PCMs [16]. Bismuth and lead were incorporated into mesoporous carbon matrices, thus preventing the leakage and agglomeration of the molten metals [17]. It is worth noting that the metal can be encapsulated into its own oxide. For example, Al nanoparticles covered with an Al_2O_3 shell were investigated by Sun et al. [18]. Metallic Bi was also impregnated into various mesoporous silica matrices, resulting in composites with shape stability and protection from oxidation [19]. Nanoparticles containing Ge, Se or their alloys embedded into a SiO_2 matrix have also been reported [20]. Al-Si alloys were encapsulated into an alumina matrix from an Al-Bi mixture used in hydrogen generation [21]. The possibility of obtaining metallic Bi/ Bi_2O_3 particles has not been investigated so far. The oxide layer can act as a barrier for molten metal leakage. A doping element was chosen in order to stabilize the oxide layer.

The possibility of obtaining molten Bi phase change materials encapsulated into its own oxide is investigated for the first time in this work. Zinc was used as a dopant for the bismuth oxide layer. The influence of reaction temperature and concentration was studied. All synthesis conditions yielded materials with at least ~60% wt. metallic Bi. The optimum reaction temperature of 85 °C yielded shape-stabilized materials which retained their solid shape at temperatures above the melting point of the metal. The average diameters of the Biof the Zn-doped samples were computed at 0.8–1.5 μm , while the oxide layer varied between 21 and 94 nm. The particle size and oxide layer diameter were significantly decreased with respect to undoped samples. An oxide layer thickness of at least 77 nm is sufficient for obtaining shape-stabilized phase change materials. The present results highlight a facile synthesis strategy for obtaining high-temperature heat storage materials with high volumetric energy density, based on metallic Bi.

2. Materials and Methods

2.1. Materials and Reagents

Zn acetate dihydrate, triethanol amine (TEA), $\text{Bi}(\text{NO}_3)_3 \cdot 5\text{H}_2\text{O}$, NaBH_4 , ammonium hydroxide 28%, concentrated nitric acid (67%) and ethanol were purchased from Sigma Aldrich (St. Louis, MO, USA) and used without further purification. Double-distilled water was used in all experiments.

2.2. Synthesis of Bi/ZnO Samples

The synthesis of Bi/0.5ZnO samples was carried out according to the following procedure. A total of 2.425 g $\text{Bi}(\text{NO}_3)_3 \cdot 5\text{H}_2\text{O}$ (5 mmol) was dissolved in 77 mL of double-distilled water and 2.112 mL of HNO_3 67% (1.981 g = 31.44 mmol). A total of 1.098 g $\text{Zn}(\text{CH}_3\text{COO})_2 \cdot 2\text{H}_2\text{O}$ (5 mmol) was then added under stirring. The solution's pH was adjusted to 9.0 by the addition of 17.5 mL of NH_4OH (28%; 4.459 g NH_4OH = 127.25 mmol). The reactions were kept at different temperatures (25, 70, 85, 100 °C) for 1 h under stirring and then aged statically at room temperature overnight. The white precipitate was separated by filtration, dried at 100 °C for 30 min and subsequently calcined at 550 °C for 1 h. The precipitate was reduced with 10 mL of aqueous NaBH_4 solution (9.8%, 25 mmol). The obtained solids were filtered and dried for 30 min at 100 °C. The samples were denoted as "Bi/0.xZnO(T)", where 0.x is the molar ratio of $\text{Zn}^{2+}/(\text{Bi}^{3+} + \text{Zn}^{2+})$ in the initial synthesis and *T* represents the reaction temperature (25, 70, 85, 100 °C). Two initial Zn^{2+} molar ratios were investigated (0.5 and 0.2), as the Zn^{2+} concentration could influence the doping of bismuth oxide. The reaction temperature *T* was also chosen, as it is an important parameter in the sol-gel synthesis of metal oxides.

The same quantity of $\text{Bi}(\text{NO}_3)_3 \cdot 5\text{H}_2\text{O}$ was employed for the synthesis of the Bi/0.2ZnO (85 °C) sample, while reducing the $\text{Zn}(\text{CH}_3\text{COO})_2 \cdot 2\text{H}_2\text{O}$ amount accordingly.

A sample containing only Bi was obtained in similar conditions at 25 °C and it was denoted as "Bi(25 °C)".

2.3. Characterization

Powder X-ray diffraction (XRD) analyses were recorded using a Rigaku MiniFlex II diffractometer using a Cu-K α radiation source ($\lambda = 1.5406 \text{ \AA}$) calibrated with an Al₂O₃ standard (SRM 676 A). The crystallite size was computed using the Scherrer equation with the (10 $\bar{2}$), (104) and (2 $\bar{1}$ 0) diffraction peaks of metallic Bi. Scanning electron microscopy (SEM) coupled with energy-dispersive X-ray spectroscopy (Bruker EDX) data were acquired using a Tescan Vega 3 LM electron microscope. Thermogravimetric analyses (TGAs) were carried out using a Mettler Toledo TGA/SDTA851e thermogravimeter at a heating rate of 10 °C min⁻¹ and under an air flow of 80 mL min⁻¹, and they were checked with CuSO₄·5H₂O and calcium oxalate monohydrate standards. Differential scanning calorimetry (DSC) analyses were performed using a Mettler Toledo DSC 3 calorimeter at a heating rate of 10 °C min⁻¹ and under a nitrogen flow of 200 mL min⁻¹. The DSC 3 was calibrated with In and Zn standards. Melting and freezing points were computed as onset temperatures, and they are therefore heating-rate-independent. Optical microscopy (OM), coupled with DSC, was carried out using an Olympus SC50 Optical Microscope at a frame rate of 1 image per 1 °C.

3. Results and Discussion

Samples containing metallic Bi and ZnO were obtained by co-precipitation of the two metal precursors in basic media, followed by calcination and reduction with sodium borohydride (see Section 3). The samples were denoted as “Bi/0.xZnO(T)”, where 0.x is the initial Zn molar ratio and T represents the reaction temperature. A Bi(25 °C) sample which did not contain Zn was also obtained.

3.1. Physico-Chemical Characterization

XRD measurements were carried out in order to assess the crystalline phases present in all of the samples. The main peaks associated with the presence of rhombohedral R $\bar{3}m$ metallic Bi phase could be noticed for all samples (Figure 1) [22]. The metallic Bi phase was the main phase in all samples. A secondary α -Bi₂O₃ phase was identified for all materials except Bi/0.5ZnO (100 °C). The highest relative intensities of oxide peaks were noticed for the Bi/0.5ZnO (85 °C) sample, indicating that this material contained the most α -Bi₂O₃ phase. No peaks corresponding to any ZnO phase were noticed, indicating that the zinc oxide did not form as a separate phase. The crystallite size of the metallic Bi phase was computed (Table 1). All samples exhibited crystallite sizes between 37 and 42 nm. No significant influence of the synthesis conditions on the crystallite size could be noticed (Table 1).

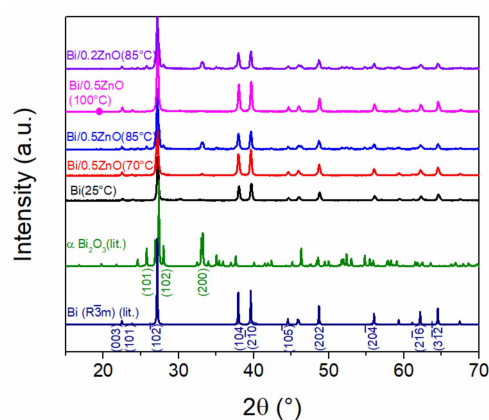


Figure 1. XRD patterns of the samples in comparison with data from the literature for α -Bi₂O₃ and rhombohedral Bi.

Table 1. Initial synthesis conditions, Zn content determined by EDX (% Zn), melting (m.p.) and freezing (f.p.) points, heat of fusion (ΔH), degree of supercooling (Sc), Bi content computed with DSC (%Bi) and crystallite size computed from the XRD data.

Sample	T ($^{\circ}\text{C}$)	Initial Bi (%wt.)	% Zn (at.)	m.p. ($^{\circ}\text{C}$) *	ΔH (Jg^{-1}) *	f.p. ($^{\circ}\text{C}$)	Sc ($^{\circ}\text{C}$)	%Bi (wt.)	Crystallite Size (nm) **
Bi/0.5ZnO (25 $^{\circ}\text{C}$)	25	72	1.0	270.2 ± 0.03	48.3 ± 0.50	226.5	43.7	90.0	40.4 ± 3.6
Bi/0.5ZnO (70 $^{\circ}\text{C}$)	70	72	1.6	270.4 ± 0.00	47.5 ± 0.13	228.2	42.2	88.0	38.6 ± 3.4
Bi/0.5ZnO (85 $^{\circ}\text{C}$)	85	72	2.9	269.6 ± 0.04	31.4 ± 0.11	223.1	46.5	58.2	38.9 ± 2.7
Bi/0.5ZnO (100 $^{\circ}\text{C}$)	100	72	1.6	269.4 ± 0.01	47.1 ± 0.02	236.3	33.1	87.1	41.9 ± 1.8
Bi/0.2ZnO (85 $^{\circ}\text{C}$)	85	91	1.5	269.9 ± 0.01	37.6 ± 0.18	229.2	40.8	69.7	37.9 ± 6.4
Bi(25 $^{\circ}\text{C}$)	25	100	-	271.4 ± 0.01	50.9 ± 0.01	227.4	44.0	94.1	37.4 ± 2.6

* Data presented as average \pm standard uncertainty. ** Computed as $\frac{0.89 \lambda}{\beta \cos \theta}$, where β is the line broadening at half of maximum intensity.

Scanning electron microscopy (SEM) images were acquired for each sample using the secondary electron detector (Figure 2). SEM measurements were used to characterize particle shapes and sizes. All materials were composed of irregular primary particles of around 1 μm , which formed larger agglomerates. The Bi/0.5ZnO (85 $^{\circ}\text{C}$) sample also contained a secondary acicular phase. The acicular particles might represent the oxide phase, in accordance with the XRD measurements. The presence of both Bi and Zn elements was confirmed and quantified through energy-dispersive X-ray spectroscopy (EDX). Successful Zn doping was noticed in all cases (Table 1). The Zn content reached a maximum of 2.9% atomic weight, versus Bi, in the sample obtained at 85 $^{\circ}\text{C}$.

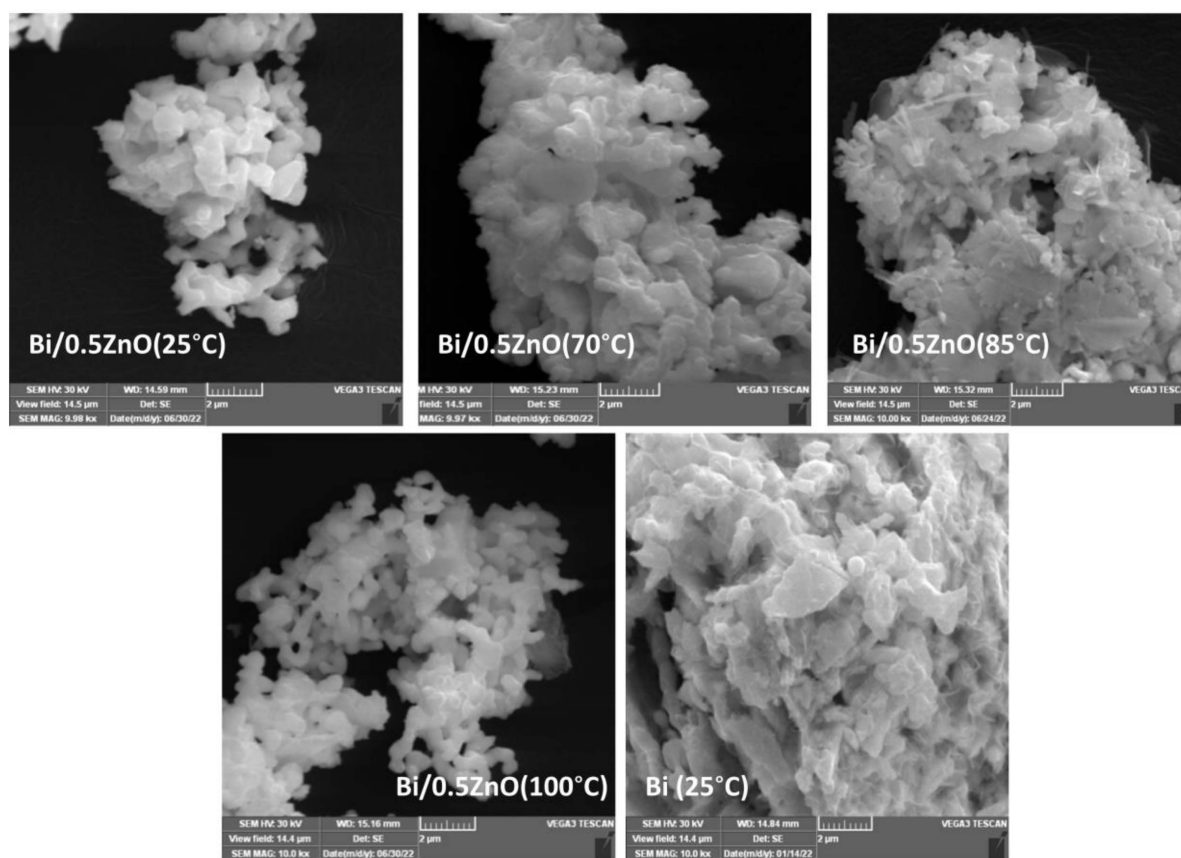


Figure 2. SEM images for the investigated samples.

3.2. Thermal Energy Storage Capacity

The melting (m.p.) and freezing (f.p.) points of the metallic Bi present in the samples and its heat of fusion were determined by differential scanning calorimetry (DSC). Heating–cooling DSC cycles were performed under nitrogen flow for all samples (Figure 3A). All materials exhibited a sharp endothermic event on heating, which was associated with the melting of metallic Bi. The m.p. and heat-of-fusion values for the pure Bi(25) sample (Table 1) were in good agreement with the literature values of bulk bismuth, at 271.4 °C and 53.1 Jg^{−1}, respectively [23]. The melting points of the composite samples were decreased by 1–2 °C in comparison with the pristine metal, which might be explained by a size-dependent reduction in the m.p. for nanometer-scale materials [19]. The freezing point (f.p.) of Bi(P) was decreased by 44 °C with respect to its melting point, indicating that supercooling occurred. Metallic bismuth is well known for its supercooling [24]. All composite samples except Bi/0.5ZnO (100 °C) also exhibited similar degrees of supercooling (Table 1). The degree of supercooling of Bi/0.5ZnO (100 °C) was lower, which might be explained by the nucleating effect of the oxide phase [24]. The freezing of liquid Bi occurred in multiple steps for all samples. This behavior is similar to other reports of Bi-containing composites [25].

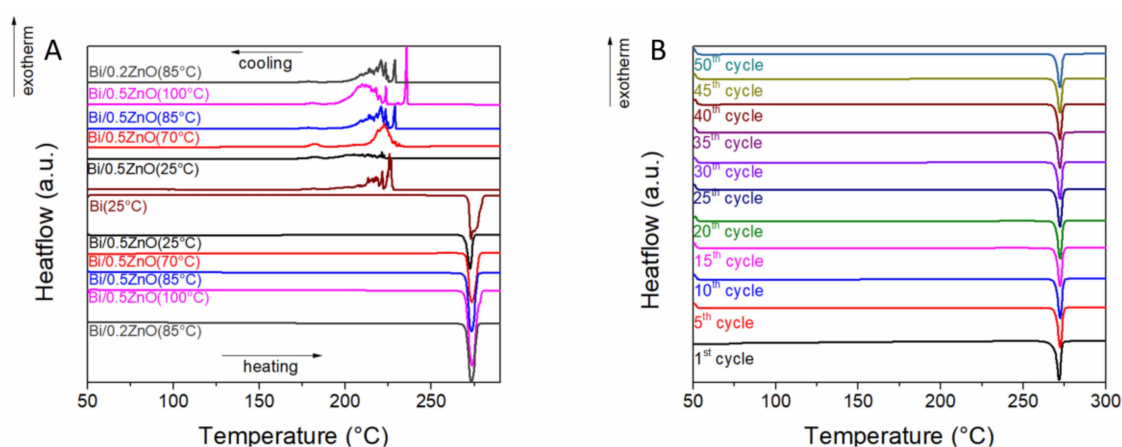


Figure 3. (A) DSC analyses of the samples and (B) thermal reliability of the Bi/0.5ZnO (85 °C) sample over 50 heating–cooling cycles.

The heat of fusion of the composites was lower than the melting enthalpy of pristine Bi (Table 1). The samples obtained at 85 °C had lower heat-of-fusion values than the other composites, indicating that they contained a higher fraction of Zn-doped Bi₂O₃. These results correlate with the XRD data, which showed higher-intensity oxide peaks for the samples obtained at 85 °C. The weight fraction of metallic Bi was computed from the melting enthalpy of the composites (Table 1). The samples obtained at 25, 70 or 100 °C contained more than 90% wt. metal. The Bi/0.5ZnO (85 °C) sample had the lowest metal content, at 61.9% wt. The presence of the oxide phase can act as a reinforcing structure, preventing molten metal leakage.

The thermal reliability of the samples was investigated through 50 heating–cooling cycles. Every fifth heating–cooling cycle was recorded. Thermal reliability represents the capacity of the samples to retain their heat storage potential during use. No significant changes in the melting points were noticed over the thermal cycles (Figure 3B). The heat-of-fusion values for the Bi(25 °C) sample remained unchanged over the course of 50 heating–cooling cycles (Figure 4). The composite materials exhibited a slight reduction in enthalpy over the thermal cycles, which could be attributed to metal oxidation or adsorption into the oxide layer (Figure 4).

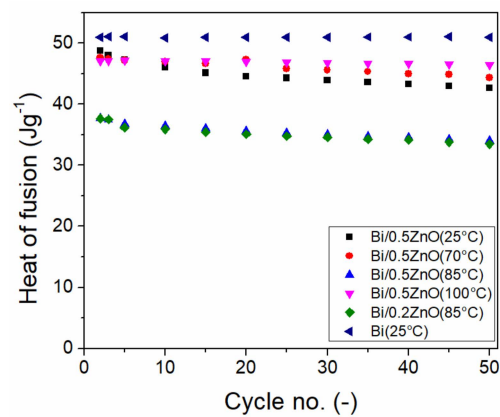


Figure 4. Thermal reliability of the Bi-containing samples over 50 heating–cooling cycles.

The Bi/0.5ZnO (85 °C) and Bi(25 °C) samples were investigated by XRD and SEM after 50 heating–cooling cycles (Figure 5). An increase in the diffraction lines associated with the oxide phases and a decrease in the peaks of metallic Bi were noticed for both samples. The SEM micrographs showed an increase in the acicular particles present on the surface of the material, which could be associated with an increase in the oxide phase. Thus, the heat storage decrease can be explained by partial oxidation of the materials on their surface.

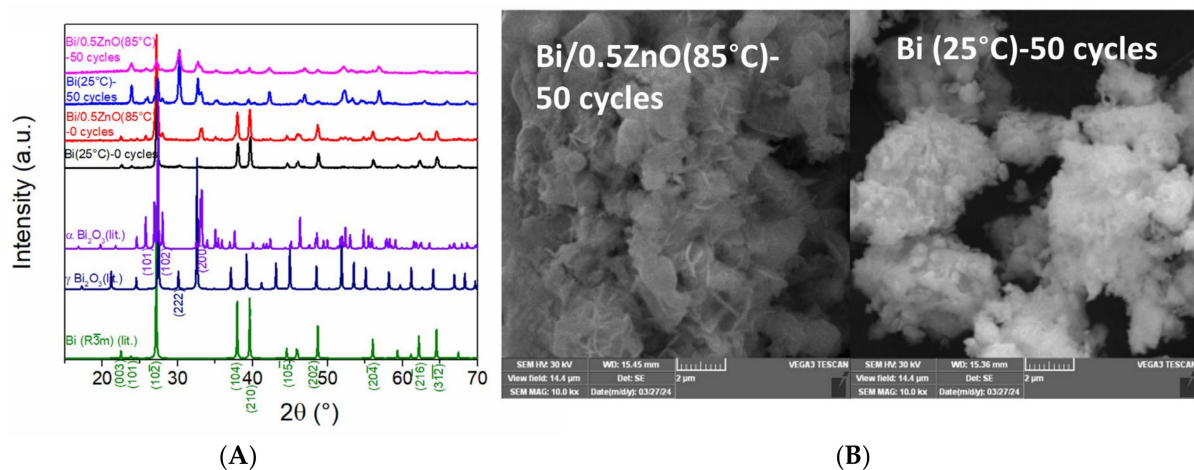


Figure 5. (A) Comparison of XRD patterns before and after 50 heating–cooling cycles with the reference patterns of Bi, α -Bi₂O₃ and γ -Bi₂O₃ and (B) SEM images after thermal reliability testing for the Bi/0.5ZnO (85 °C) and Bi(25 °C) samples.

An important property of composite phase change materials is their shape stability—the ability of the material to retain its solid macroscopic shape above its melting point. Shape stability prevents leakage of the metal, which can cause a loss of thermal energy storage during use. High-temperature optical microscopy, coupled with DSC, was used to investigate the shape stability of the Bi-containing materials (Figure 6). The samples were prepared as pellets and heated from room temperature to temperatures above the melting point of the metal. The samples retained their overall shape when heated from 50 to 300 °C. The leakage of molten Bi was noticed for all samples except Bi/0.5ZnO (85 °C). The leaked metal was able to be seen as spherical particles which formed on the surface of the samples after thermal treatment. The Bi/0.5ZnO (85 °C) sample contained a higher fraction of oxides, which might explain its shape stability.

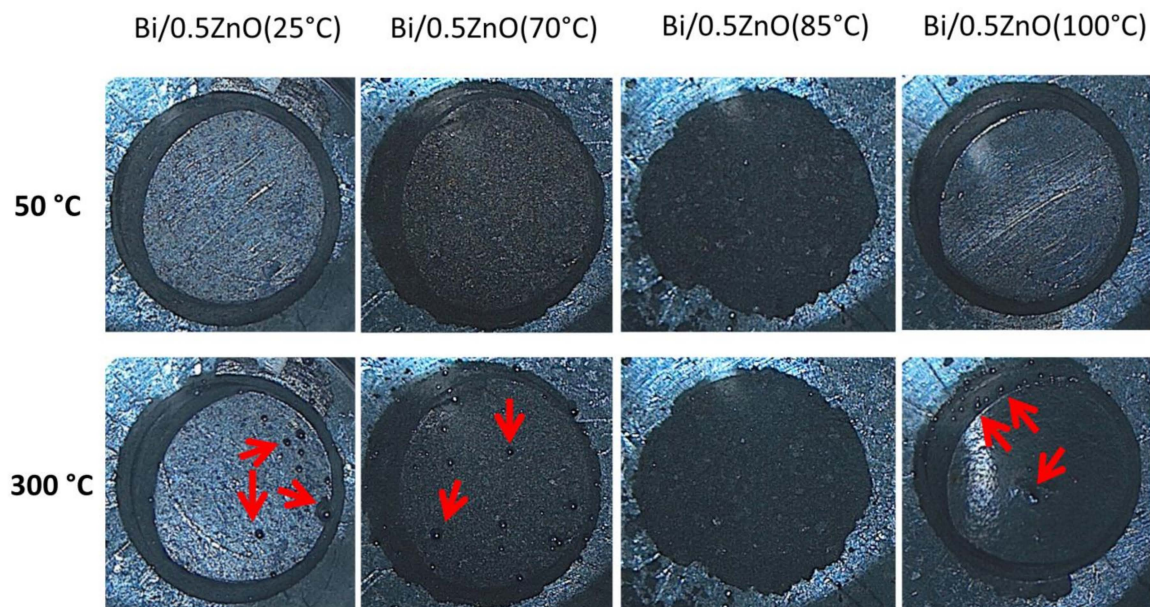


Figure 6. Optical microscopy images of the samples taken at 50 °C (**top**) and 300 °C (**bottom**). The red arrows are visual aids, pointing towards the leaked molten Bi.

The shape stability of the Bi/0.5ZnO (85 °C) sample was also investigated after 50 heating–cooling cycles. The material retained its macroscopic solid shape after the thermal reliability cycles (Figure 7). The amount of Zn was conserved after 50 heating–cooling cycles (Figure 8).

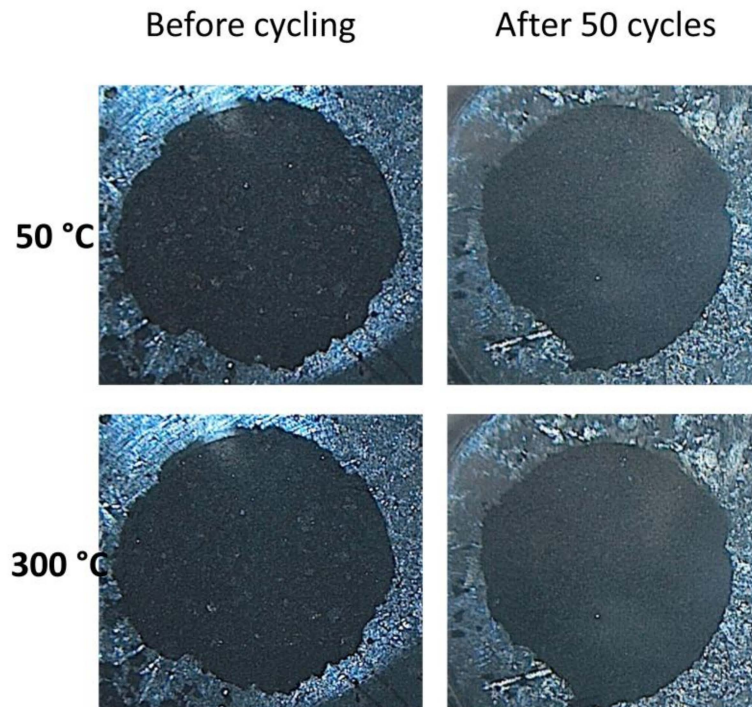


Figure 7. Optical microscopy images of the Bi/0.5ZnO (85 °C) sample, taken at 50 °C (**top**) and 300 °C (**bottom**) before (**left**) and after (**right**) 50 heating–cooling cycles.

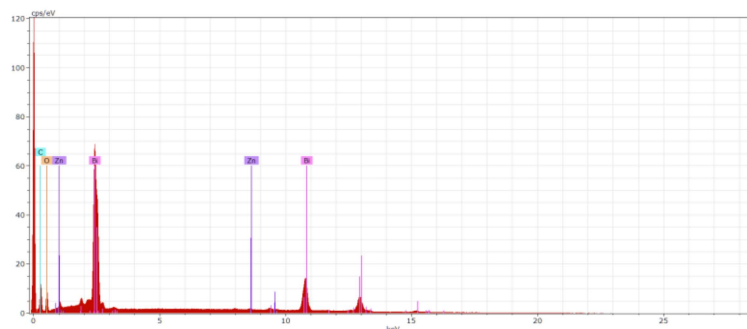


Figure 8. EDX spectra of the Bi/0.5ZnO (85 °C) sample after 50 heating-cooling cycles.

The melting points of the composite samples were decreased with respect to bulk metal or the Bi(25 °C) sample. The melting point change is a consequence of reduced vapor pressure over the liquid phase in capillaries [26]. The melting point decrease (ΔT) is proportional to the particle diameter, and it was quantified with the Gibbs–Thomson equation (Equation (1)). The Gibbs–Thomson equation is derived from the Kelvin and Clausius–Clapeyron equations, and it does not take into account the effects of pressure under isochoric conditions. It is worth noting that a fully confined liquid phase will experience increased pressure due to the positive changes in the molar volume, leading to higher melting points. An m.p. decrease was also noticed for aluminum nanoparticles coated in a thin layer of aluminum oxide [18].

$$\Delta T = T(\infty) - T(r) = -\frac{T(\infty) \cdot M \cdot \gamma_{sl}}{\rho \cdot \Delta H_f} \cdot \frac{\alpha}{r} \cos \theta = \frac{K}{r} \quad (1)$$

where $T(\infty)$ and $T(r)$ are the melting points of the bulk and particles with an average radius r , M is the molar mass, ρ is the density, γ_{sl} represents the solid–liquid surface tension, ΔH_f is the heat of fusion, α is a shape parameter of the confined phase and θ is the contact angle between the liquid metal and the oxide, which is typically assumed to be 180°. K is a term that contains all the constants, and it is equal to 826.9 nm in this case [27].

The average particle diameter was estimated using Equation (1) and the experimentally determined m.p. values (Table 2). The effect of pressure on the Bi melting transition was not considered. The data showed that all composites had average particle diameters between 0.70–1.50 μm , while the Bi(25 °C) sample had larger average particles, at 16.5 μm . The computed diameters were in good agreement with the SEM analyses.

Table 2. Bi, Bi₂O₃ and ZnO weight fractions and average Bi particle diameters (d) computed with the Gibbs–Thomson equation and thickness of oxide layer (t).

Sample	Bi (% wt.)	Bi ₂ O ₃ (% wt.)	ZnO (% wt.)	d (μm)	t (nm)
Bi/0.5ZnO (25 °C)	90.0	9.6	0.4	1.27	25
Bi/0.5ZnO (70 °C)	88.0	11.4	0.6	1.50	37
Bi/0.5ZnO (85 °C)	58.2	40.7	1.1	0.87	94
Bi/0.5ZnO (100 °C)	87.1	12.3	0.6	0.79	21
Bi/0.2ZnO (85 °C)	69.7	29.8	0.5	1.10	77
Bi(25 °C)	94.1	5.9	0.0	16.5	186

The composition of each sample could then be estimated from the metallic Bi weight fraction, as determined by DSC, and the Zn/Bi atomic ratio, which was computed from the EDX analyses (Table 2). The composition estimation was then used to calculate the average thickness of the oxide layer (Equation (2)) [18]. The thickness was computed as the difference between the average particle diameters, which were computed from the

mass composition and density of each phase, and the average metallic Bi diameter using Equation (2).

$$2t = d_{Bi} \left(\sqrt[3]{\frac{\frac{m_{Bi}}{\rho_{Bi}} + \frac{m_{Bi_2O_3}}{\rho_{Bi_2O_3}} + \frac{m_{ZnO}}{\rho_{ZnO}}}{\frac{m_{Bi}}{\rho_{Bi}}} - 1} \right) \quad (2)$$

where t is the average oxide layer thickness, d_{Bi} is the average metallic Bi diameter (Table 1) and m and ρ are the mass fraction and density of the Bi, Bi_2O_3 or ZnO phases.

The samples prepared at 85 °C had greater oxide layer thicknesses (77–94 nm), while the other composites had average thickness values between 21 and 37 nm. The lower thickness values could indicate incomplete oxide coverage of the metal particles and thus explain the leakage of the molten Bi noticed during the optical microscopy measurements (Table 2). The Bi(25 °C) sample exhibited the largest value for the average Bi oxide layer thickness, at 186 nm. Overall, the composites showed that a 77 nm average oxide layer thickness was sufficient to prevent the leakage of molten Bi, yielding shape-stabilized PCMs.

The samples obtained in this work at a synthesis temperature of 85 °C and with a 0.2 or 0.5 Zn/(Zn+Bi) initial molar ratio compared favorably with previously reported shape-stabilized Bi composites (Table 3). The samples exhibited high metal loading, shape-stability and increased heat-of-fusion values in comparison with previous literature reports.

Table 3. Comparison between the thermal energy storage properties of the samples reported in this work and materials previously reported in the literature. Heat-of-fusion values are expressed in J per g of composite sample.

Samples	Bi (% wt.)	m.p. (°C)	ΔH (Jg ⁻¹)	Shape Stability	Reference
Bi nanoparticles/PI	19.8	240	8.34	Yes	[28]
Bi nanoparticles/Ag	34.1	252	12.82	Yes	[25]
Bi/FDU-12 mesoporous silica	50	269.9	21.9	Yes	[27]
Bi/mesocellular foam silica	61	268.6	32.1	Yes	[19]
Bi/C	48	239	16.9	Yes	[17]
Bi/Bi ₂ Zn _x O _{3+x}	69.7	269.9	37.6	Yes	This work

4. Conclusions

Shape-stabilized phase change materials based on metallic bismuth were obtained with the aim of reversibly storing heat at elevated temperatures through the melting–freezing phase transition. Zinc acetate was added to the initial synthesis solution in order to create a protective mixed oxide layer, which was able to confine the molten metal, preventing its leakage. The samples were obtained through the precipitation of Zn and Bi precursors in basic media, followed by calcination and chemical reduction. The influences of the initial synthesis temperature and the Bi/Zn molar ratio were investigated.

All synthesis conditions yielded materials containing at least 60% wt. metallic Bi, surrounded by a layer of Zn-doped Bi_2O_3 . The metallic Bi phase had an average particle diameter of 0.8–1.5 μm , while the oxide layer varied between 21 and 94 nm. Samples containing at least 31% wt. oxides retained their solid shape, preventing liquid Bi melting. These samples were obtained at an initial synthesis temperature of 85 °C. The oxide layer thickness was estimated at 77–94 nm. The samples were able to reversibly store thermal energy through the melting and freezing of the metal in the 220–270 °C temperature range. Their heat storage capacity varied between 37–49 Jg⁻¹.

The results show that shape-stabilized phase change materials containing metallic bismuth as the active heat storage stage and a zinc-doped bismuth oxide layer can be obtained and used to reversibly store heat above 200 °C.

Author Contributions: Conceptualization, R.-A.M.; methodology, C.M.V. and R.-A.M.; formal analysis, D.L., D.B., C.M. and R.-A.M.; investigation, C.M.V., D.L., D.B., C.M. and R.-A.M.; writing—original draft preparation, C.M.V. and R.-A.M.; writing—review and editing, C.M.V. and R.-A.M.; visualization, C.M.V. and R.-A.M.; supervision, R.-A.M.; project administration, R.-A.M.; funding acquisition, R.-A.M. All authors have read and agreed to the published version of the manuscript.

Funding: This work was supported by a grant from the Romanian Ministry of Education and Research, CNCS-UEFISCDI, project number: PN-III-P1-1.1-TE-2019-1456, TE No. 166/2020, within PNCDI III.

Data Availability Statement: The raw data supporting the conclusions of this article will be made available by the authors on request.

Conflicts of Interest: The authors declare no conflicts of interest.

References

1. Cekirge, H.M.; Erturan, S.E.; Thorsen, R.S. The CSP (Concentrated Solar Power) Plant with Brayton Cycle: A Third Generation CSP System. *Am. J. Mod. Energy* **2020**, *6*, 43–50. [[CrossRef](#)]
2. Zhao, Y.; Zhao, C.Y.; Markides, C.N.; Wang, H.; Li, W. Medium- and high-temperature latent and thermochemical heat storage using metals and metallic compounds as heat storage media: A technical review. *Appl. Energy* **2020**, *280*, 115950. [[CrossRef](#)]
3. Mitran, R.-A.; Ioniță, S.; Lincu, D.; Berger, D.; Matei, C. A Review of Composite Phase Change Materials Based on Porous Silica Nanomaterials for Latent Heat Storage Applications. *Molecules* **2021**, *26*, 241. [[CrossRef](#)] [[PubMed](#)]
4. Zhang, P.; Xiao, X.; Ma, Z.W. A review of the composite phase change materials: Fabrication, characterization, mathematical modeling and application to performance enhancement. *Appl. Energy* **2016**, *165*, 472–510. [[CrossRef](#)]
5. Geissbühler, L.; Kolman, M.; Zanganeh, G.; Haselbacher, A.; Steinfeld, A. Analysis of industrial-scale high-temperature combined sensible/latent thermal energy storage. *Appl. Therm. Eng.* **2016**, *101*, 657–668. [[CrossRef](#)]
6. Aftab, W.; Huang, X.; Wu, W.; Liang, Z.; Mahmood, A.; Zou, R. Nanoconfined Phase Change Materials for Thermal Energy Applications. *Energy Environ. Sci.* **2018**, *11*, 1392–1424. [[CrossRef](#)]
7. Hidaka, H.; Yamazaki, M.; Yabe, M.; Kakiuchi, H.; Ona, E.P.; Kojima, Y.; Matsuda, H. New PCMs prepared from erythritol-polyalcohols mixtures for latent heat storage between 80 and 100 C. *J. Chem. Eng. Jpn.* **2004**, *37*, 1155–1162. [[CrossRef](#)]
8. Garay Ramirez, B.M.L.; Glorieux, C.; San Martin Martinez, E.; Flores Cuautle, J.J.A. Tuning of thermal properties of sodium acetate trihydrate by blending with polymer and silver nanoparticles. *Appl. Therm. Eng.* **2014**, *62*, 838–844. [[CrossRef](#)]
9. Marske, F.; Martins de Souza e Silva, J.; Wehrspohn, R.B.; Hahn, T.; Enke, D. Synthesis of monolithic shape-stabilized phase change materials with high mechanical stability via a porogen-assisted in situ sol-gel process. *RSC Adv.* **2020**, *10*, 3072–3083. [[CrossRef](#)]
10. Mitran, R.A.; Berger, D.; Matei, C. Phase Change Materials Based on Mesoporous Silica. *Curr. Org. Chem.* **2018**, *22*, 2644–2663. [[CrossRef](#)]
11. Wang, Y.; Song, Y.; Li, S.; Zhang, T.; Zhang, D.; Guo, P. Thermophysical properties of three-dimensional palygorskite based composite phase change materials. *Appl. Clay Sci.* **2020**, *184*, 105367. [[CrossRef](#)]
12. Chang, C.; Nie, X.; Li, X.; Tao, P.; Fu, B.; Wang, Z.; Xu, J.; Ye, Q.; Zhang, J.; Song, C.; et al. Bioinspired roll-to-roll solar-thermal energy harvesting within form-stable flexible composite phase change materials. *J. Mater. Chem. A* **2020**, *8*, 20970–20978. [[CrossRef](#)]
13. Qi, H.; Zhang, T.; Zhang, D.; Wang, K.; Wang, Y. Paraffin/chitosan composite phase change materials fabricated by piercing-solidifying method for thermal energy storage. *AIP Adv.* **2020**, *10*, 035218. [[CrossRef](#)]
14. Fukahori, R.; Nomura, T.; Zhu, C.; Sheng, N.; Okinaka, N.; Akiyama, T. Thermal analysis of Al-Si alloys as high-temperature phase-change material and their corrosion properties with ceramic materials. *Appl. Energy* **2016**, *163*, 1–8. [[CrossRef](#)]
15. Zhang, F.; Zhong, Y.; Yang, X.; Lin, J.; Zhu, Z. Encapsulation of metal-based phase change materials using ceramic shells prepared by spouted bed CVD method. *Sol. Energy Mater. Sol. Cells* **2017**, *170*, 137–142. [[CrossRef](#)]
16. Hsu, T.-H.; Chung, C.-H.; Chung, F.-J.; Chang, C.-C.; Lu, M.-C.; Chueh, Y.-L. Thermal hysteresis in phase-change materials: Encapsulated metal alloy core-shell microparticles. *Nano Energy* **2018**, *51*, 563–570. [[CrossRef](#)]
17. Tran, N.; Zhao, W.; Carlson, F.; Davidson, J.H.; Stein, A. Metal Nanoparticle-Carbon Matrix Composites with Tunable Melting Temperature as Phase-Change Materials for Thermal Energy Storage. *ACS Appl. Nano Mater.* **2018**, *1*, 1894–1903. [[CrossRef](#)]
18. Sun, J.; Simon, S.L. The melting behavior of aluminum nanoparticles. *Thermochim. Acta* **2007**, *463*, 32–40. [[CrossRef](#)]
19. Lincu, D.; Ioniță, S.; Trică, B.; Culita, D.C.; Matei, C.; Berger, D.; Mitran, R.-A. Bismuth-mesoporous silica-based phase change materials for thermal energy storage. *Appl. Mater. Today* **2022**, *29*, 101663. [[CrossRef](#)]
20. Shin, S.J.; Guzman, J.; Yuan, C.W.; Liao, C.Y.; Boswell-Koller, C.N.; Stone, P.R.; Dubon, O.D.; Minor, A.M.; Watanabe, M.; Beeman, J.W.; et al. Embedded binary eutectic alloy nanostructures: A new class of phase change materials. *Nano Lett.* **2010**, *10*, 2794–2798. [[CrossRef](#)]
21. Wei, H.; Qiu, C.; Wang, C.; Lin, K.; Yang, S.; Han, J.; Lu, Y.; Liu, X. Development of phase change materials using hydrolyzed Al-Bi composite powder for solar energy storage. *Chem. Eng. J.* **2021**, *421*, 127836. [[CrossRef](#)]

22. Krüger, J.; Winkler, P.; Lüderitz, E.; Lück, M.; Wolf, H.U. Bismuth, Bismuth Alloys, and Bismuth Compounds. In *Ullmann's Encyclopedia of Industrial Chemistry*; Wiley: Hoboken, NJ, USA, 2003. [[CrossRef](#)]
23. Archer, D.G. Enthalpy of Fusion of Bismuth: A Certified Reference Material for Differential Scanning Calorimetry. *J. Chem. Eng. Data* **2004**, *49*, 1364–1367. [[CrossRef](#)]
24. Bramfitt, B.L. A Study of the Supercooling Behavior of High Purity Liquid Bismuth. Ph.D. Thesis, University of Missouri at Rolla, Rolla, MO, USA, 1966.
25. Liu, M.; Ma, Y.; Wu, H.; Wang, R.Y. Metal Matrix–Metal Nanoparticle Composites with Tunable Melting Temperature and High Thermal Conductivity for Phase-Change Thermal Storage. *ACS Nano* **2015**, *9*, 1341–1351. [[CrossRef](#)] [[PubMed](#)]
26. Hugo, K.C. Confinement effects on freezing and melting. *J. Phys. Condens. Matter* **2001**, *13*, R95.
27. Mitran, R.-A.; Lincu, D.; Berger, D.; Matei, C. FDU-12 cubic mesoporous silica as matrix for phase change materials using bismuth or stearic acid. *J. Therm. Anal. Calorim.* **2022**, *147*, 14097–14106. [[CrossRef](#)]
28. Liu, M.; Wang, R.Y. Phase change nanocomposites with tunable melting temperature and thermal energy storage density. *Nanoscale* **2013**, *5*, 7234–7237. [[CrossRef](#)]

Disclaimer/Publisher's Note: The statements, opinions and data contained in all publications are solely those of the individual author(s) and contributor(s) and not of MDPI and/or the editor(s). MDPI and/or the editor(s) disclaim responsibility for any injury to people or property resulting from any ideas, methods, instructions or products referred to in the content.